Structural Investigation of *Vinca* Domain Tubulin Binders by Pharmacophore, Atom based QSAR, Docking and Molecular Dynamics Simulations

Mohd Athar[a,*], Mohsin Y. Lone[a], Vijay M. Khedkar[b,c], Ashish Radadiya[d], Anamik Shah[d,e], and Prakash C. Jha[f,*]

[a]*School of Chemical Sciences, Central University of Gujarat, Gandhinagar 382030, Gujarat, India;* [b]*School of Health Sciences, Discipline of Pharmaceutical Sciences, University of KwaZulu-Natal, Westville, Durban 4000, South Africa;* [c]*Department of Pharmaceutical Chemistry, Shri Vile Parle Kelavani Mandal's Institute of Pharmacy, Mumbai - Agra National Hwy, Dhule, Maharashtra 424001, India* [d]*National Facility for Drug Discovery Complex, Department of Chemistry, Saurashtra University, Rajkot 360005, Gujarat, India;* [e]*Gujarat Vidyapith, Ahmedabad 380014, Gujarat, India;* [*f]*Centre for Applied Chemistry, Central University of Gujarat, Gandhinagar 382030, Gujarat, India*

Abstract: ***Aim and Objective*****:** *Vinca* domain of tubulin protein is the potential target for different microtubule targeting drugs (MTD). However, its binding mechanism and structure-activity-relationship (SAR) is not well understood in terms of ligand-receptor interactions and structure functionality requirements. This limits the exploitation of vinca domain for developing novel clinical leads. Herein, as a progressive step towards the exploration of this target, we rendered the *in-silico* insight through the development of a robust pharmacophore model followed by the QSAR, Molecular Docking and Molecular Dynamics (MD) simulations. Furthermore, the study was undertaken to identify potent inhibitors that can inhibit vinca domain of tubulin.

Materials and Methods**:** Utilizing the well-defined tubulin polymerization inhibition activities, common pharmacophore hypotheses were constructed and scored for their rankings. The hypotheses were validated by 3D-Atom based QSAR and tested for various statistically relevant metrices. Thereafter, virtual screening was performed with ZINC natural product database and the screened *hits* were evaluated for structure-based studies *via* molecular docking and molecular dynamics simulations.

Results**:** The predictive 3D-QSAR based pharmacophore model consists of two hydrogen bond acceptors (A), two hydrogen bond donors (D) and one hydrophobic (H) group. Significance of the model was reflected from the statistical parameters *viz.* $r^2 = 0.98$, $q^2 = 0.72$, F = 562.9, RMSE = 0.11 and Pearson-R = 0.87. Further, the docking scores of the retrieved *hits* deciphered that the ligands were adequately bound in the pocket. Moreover, RMSD fluctuations of protein (1.0 to 1.75A) and ligand (0.3 to 2.3 Å) in molecular dynamics simulations insinuate towards the conformational and interactions stability of the complexes.

Conclusion**:** The quantitative pharmacophore model was developed from range of natural product scaffolds in order to incorporate all the complimentary features accountable for inhibition. The obtained *hits* were found to occupy similar binding region and superimpose well over the reference ligand. Therefore, it can be concluded that hierarchical combination of methods exploited in this study can steer the identification of novel scaffolds. Moreover, the rendered hit molecules could serve as potential inhibitory leads for the development of improved inhibitors targeting *Vinca* domain.

Keywords: Pharmacophore, microtubules, antimitotic, virtual screening, natural products, molecular docking, QSAR.

1. INTRODUCTION

Microtubule targeting drugs (MTD) are characterized by a variety of compounds targeted against microtubular proteins that form major structural components of the cell [1]. These microtubules are highly dynamic hollow cylindrical polymers composed of α, β-tubulin globular protein subunits vital for the cellular proliferation, signaling and for the cellular movements [2]. Despite forming major cytoskeleton component, it plays key role in intracellular transportation, maintaining cellular shape, and in cell division [3]. Attributable to the multifarious biological

*Address correspondence to these authors Centre for Applied Chemistry, Central University of Gujarat, Gandhinagar 382030, Gujarat, India; Tel: +918866823510; E-mail: prakash.jha@cug.ac.in (P.C.J), School of Chemical Sciences, Central University of Gujarat, Gandhinagar 382030, Gujarat, India; E-mail: mathar93@gmail.com (M.A)

implications, it exemplifies as potential pharmaceutical target for diverse group of anti-parasitic and anticancer drugs [4]. It can also be argued that microtubules represent as the only single best non-DNA cancer target identified till date [1, 5, 6]. Hence, for boosting the advances in anticancer therapy, research for microtubule/tubulin therapeutics is of central contour [7-9]. The three-dimensional structure of tubulin protein consists of two internal β-sheets surrounded by several α-helices arranged parallel to the cylindrical axis and forms a stable heterodimer [10]. It undergoes polymerisation by nucleation-elongation mechanism and exhibits dynamics with the expense of energy provided from the GTP hydrolysis at the N-terminal [11, 12].

In particular, the microtubule dynamic (tread milling and dynamic instability) execute critical role in the polymeric assembly and functioning of mitotic spindle. Specifically, rapid dynamic microtubules are obligate for the orchestration of mitotic events like congression, equipartitioning and chromosomal bipolar alignment. This essential dynamic equilibrium is affected by treatment of agents that can shift equilibrium between polymerisation and depolymerisation phases [13]. Hence, subsequent binding of drugs with tubulin attenuates microtubule stability, dynamics and other functions including inhibition of mitosis during metaphase/anaphase stage. This in turn led to halting of the cellular transition by suppressing spindle dynamics followed by mitotic blockage and cellular apoptosis [14]. Likewise, a large number of chemically diverse compounds have been developed as a potential class of chemotherapeutic drugs against cancer [15-17]. Intriguingly, targeting of such drugs can be originated via three possible ways/sites (1) *Vinca* domain (depolymerization) (2) colchicine site; or (3) taxane site (depolymerisation inhibitor) [18]. Vinca domain is represented by inter-dimeric space between β-subunit of one dimer and α-subunit of another dimer. However, colchicine domain is well explored and targeted by ligands like colchicine, combrestatin, 2-methoxy estradiol etc. The third, taxane site is typified by drugs like taxanes, paclitaxel and docetaxel that bind to the lumen of the β -subunit of the polymerized microtubules [19].

Vinca binders are specifically classified into ″*Vinca* site″ binders and ″peptide site″ binders in the *Vinca* domain of tubulin [20]. Vinca site comprise of vinblastine, vincristine, vinorelbine *etc*. and peptide site represented by dolastatins, hemisterlins, helichondrins *etc*. Based on competitive and noncompetitive mode of action, the vinca alkaloids can be further categorized into various classes as mentioned in Fig. (**1**) [12, 21, 22].

Among the clinical MTD, most drugs are presumed to bind with colchicine domain, as the understanding of the *Vinca* domain is still obscurely explored. Owing to the increasing menace of drug resistance, toxicity and other side effects of MTDs, there is an urgent need to map vinca domain for developing new therapeutics [13, 23, 24].

It is also important to mention that there are various studies that attempted to model and design antimitotic compounds [25-28]. However, such studies did not address the complicacy of vinca site. The present study has been carried out with diverse scaffolds to generate pharmacophore model and for screening antimitotic/anticancer compounds. Taking into account the dominance of natural product based known tubulin inhibitors [29], ZINC natural product database [30, 31] was used in the present study. Distinctly, to avoid any uncertainties associated with model building, modelling has been carried using the polymerisation inhibition activities of pure tubulin protein (IC_{50}). The study would be certainly useful for opening new vistas to design new antimitotic and anticancer therapeutic. To the best of our knowledge, this is the first pharmacophore based 3D-QSAR study of *Vinca* binders.

2. MATERIALS AND METHODS

2.1. Computational Details

Pharmacophore modelling and ligand based virtual screening studies were carried out using PHASE, version 4.1 [32, 33] module incorporated in Schrödinger Suite 2014-4 [34] installed on High Performance Computing system of 48 Xenon core with CentOS operating system. Discovery Studio v4.0 was used to clean and minimize the *hits* that were subsequently imported for FlexX docking on LeadIt 2.1.8 [35].

2.1.1. Dataset of Vinca Binders

Literature and databases search divulge the substantial evidences of only 26 compounds with well-defined tubulin polymerization inhibition activities (IC_{50}) (Fig. **S1**). The limited but structurally diverse dataset was selected based on the following criteria: (1) all compounds with inhibitory activity specifically against tubulin proteins and their binding at Vinca domain of tubulin, (2) similar biological assay

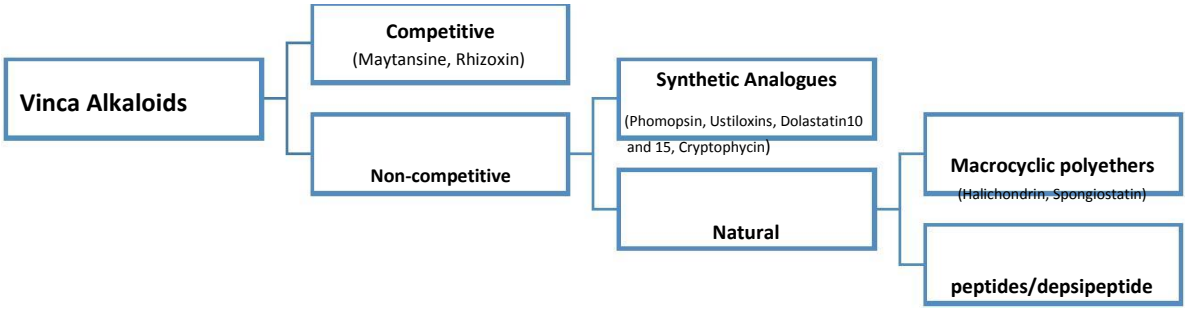

Fig. (1). Depiction of various classes of *Vinca* alkaloids targeting *Vinca* site of the tubulin protein [12, 15, 16].

conditions; and (3) ligands may act competitively or non-competitively with the binding of other Vinca alkaloid. Thereafter, experimental activities (IC_{50}) were converted to molar units and further to the negative logarithmic unit by converting into the pIC_{50} by employing Equation 1.

Eq.1

where, IC_{50} is the micro molar concentration of the inhibitor producing 50% inhibition. The obtained pIC_{50} values were considered as the dependent variable throughout the modelling studies (Table **1**).

2.1.2. Processing of Chemical Structures

The structure of the compounds were sketched using the *builder* panel in Maestro followed by cleaning and optimization using *Ligprep* [36] module that performs addition of hydrogens, adjusts bond length and angles, checks for the chiralities, tautomers, stereochemistries and ring conformations. The atomic charges were assigned by Optimized Potential for Liquid Simulations (OPLS-2005) force field [37] and possible ionisation states were generated at a pH of 7.0. The *ConfGen* module integrated in PHASE was used to generate energy minimized bioactive conformers with OPLS-2005 force field at a cut-off RMSD of 1.0Å [38]. Conformers were also filtered through a relative energy window of 104.6 kJ/mol, with the considerations of 1000 maximum number of conformers and pre-and post-minimization steps of 1000 per ligand.

Table 1. Dataset of *Vinca* domain binders extracted from literature with their activity of tubulin polymerization.

No.	Compounds	IC50(μm)	References
1.	Vinblastine	1.7	[39]
2.	Vincristine	1.7	[39]
3.	Vindesine	1.4	[39]
4.	Vinfosiltine	2.4	[39]
5.	Vinorelbine	1.7	[39]
6.	Vinflunine	3.1	[39]
7.	Dolastatin 10	1.2	[40]
8.	Dolastatin 10 (Isomer 2)	1.4	[40]
9.	Dolastatin 10 (Isomer 5)	2.6	[40]
10.	Dolastatin 10 (Isomer 8)	28	[40]
11.	Dolastatin 10 (Isomer 15)	40	[40]
12.	Dolastatin 15	23	[40]
13.	ER-076349	5.7	[41]
14.	EribulinMesylate (E7389)	11	[42]
15.	E7974(hemisterlinanalog)	3.9	[43]
16.	ER-809878(hemisterlinanalog)	4.8	[43]
17.	EV-812906(hemisterlinanalog)	2.2	[43]
18.	Sablidotin (TZT-1027)	2.2	[44]
19.	Halichondrin B	7.2	[45]
20.	Homohalichondrin B	20	[45]
21.	Cryptophycin 1	2.7	[46]
22.	Diazonamide A	0.33	[46]
23.	Phompsin A	1.4	[45]
24.	Maytansine	3.4	[45]
25.	Rhizoxin	6.9	[45]
26.	Spongistatin	3.6	[47]

* Inhibition Of Tubulin Polymerization IC_{50} (μm)

2.1.3. Pharmacophore Model Generation

Ligand based 3D-Pharmacophore model was developed to identify the minimal fundamental pharmacophoric features that govern the biological activity. Before the model building, the ligands were categorized into actives and inactives by applying proper threshold in terms of activity and structural diversity. Six active and five inactive molecules were ascribed. Importantly, the inactive compounds are used to validate the generated hypotheses as their features does not dictate for any activity [48]. However, inactive set was used to adjust the hypothesis scores that reflect the quality of the model [49].

2.1.3.1. Creating Pharmacophore Sites

A set of pharmacophoric features are used to represent ligand structure and a set of site points in 3D space to develop a common pharmacophore hypothesis (CPH). These site points are characterized by type, location and directionality [32]. Moreover, site points represent various chemical features that possibly facilitate the non-covalent binding of ligand to the target. PHASE uses six types of built-in pharmacophoric features: H-bond donor (D), H-bond acceptor (A), hydrophobic group (H), negatively charged group (N), positively charged group (P), and aromatic ring (R). All pharmacophoric sites are internally signified by a set of SMARTS pattern and assigned one of the three possible geometric representations: point, group or vector [50]. However, *feature definition* rules are applied to map the positions of the pharmacophore sites.

2.1.3.2. Generating Common Pharmacophores

A set of active ligands and their conformations were used to build the 3D pharmacophore model (active analog approach) [51]. As per the IUPAC recommendations, a pharmacophore is ″the ensemble of steric and electronic features that is necessary to ensure the optimal supramolecular interactions with a specific biological target structure and to trigger (or to block) its biological response″[52]. Therefore, to augment the stereo-electronic features in the form of pharmacophore model, PHASE algorithm was used. It is based on analyzing *k*-point pharmacophores culled from the conformations of actives constraining to match on to all k-sites [32]. Common *k*-point pharmacophore feature were perceived from a set of variants (set of feature types) and from different subset of actives using tree-based partitioning method that assembles similar pharmacophores on the basis of their inter-site distances, *i.e.,* the distances between pairs of sites in the pharmacophore.

Five-point common pharmacophore were generated with the requirement that all active ligands should match. The hypotheses were generated with inter-feature distance of 1.5Å by employing systematic variation of number of sites and number of matching active compounds.

2.1.3.3. Scoring Hypothesis

A set of hypotheses that survives in partitioning procedure within the space of intersite distances undergo scoring for conceding best alignment of active ligands. The scoring allows ranking of different hypothesis and makes rational choices among the hypothesis for further investigations. Scoring was conducted using default parameters for site, vector, and volume terms [32]. The final scoring function *i.e*., survival score contains the following terms:

$$S = W_{site}S_{site} + W_{vec}S_{vec} + W_{vol}S_{vol} + W_{sel}S_{sel} + W^{m}{}_{rem}$$

where W's are weights and S's are scores, S_{site} represents an alignment score and S_{vec} represents vector score. S_{vol} denotes volume score based on overlay of van der Waals models of non-hydrogen atoms. S_{sel} signifies the selectivity score that accounts for the number of molecules that match the hypothesis. The best common pharmacophore hypothesis was selected depending on the adjusted survival scores among all the hypotheses.

2.1.4. Pharmacophore Model Validation by 3D-QSAR

The top-scored hypothesis was used to generate atom-based 3D-QSAR model for explaining structure-activity relationship. For QSAR prediction, the dataset was randomly divided into training and test sets. In particular, test set should be a subset of the training set in terms of structural diversity and activity span. Out of 26 molecules, the dataset was randomly divided into a training set of 17 compounds and remaining in the test set. Furthermore, wide range of structural diversity of compounds in the test set legitimate us to evaluate the extrapolative accuracy of the 3D-QSAR models [53].

The QSAR models can decipher the positively and negatively contributing factors to the activity. In particular, PHASE uses grid based modeling, in which the spaces occupied by the aligned ligands were divided into cubes of typically 1Å on each side followed by binary valued occupancies (″bits″) treatment. Atom-based 3D-QSAR model was generated which treat molecule as a set of overlapping van der Waals spheres [54]. The models were generated with grid spacing set to 1Å. Thereafter, the test set molecules were aligned and their activities were predicted through the regression analysis [55]. Four factor Partial Least Squares (PLS) regression was applied during the QSAR model building. The predictive power of the model was tested for internal stability against test set compounds and examined for external validations. Internal Validation was carried out using the leave-one-out (, LOO) method employing the following equation 2.

$$\frac{\Sigma}{\Sigma}$$ Eq.2

where and are the predicted and actual activities of the *i*th molecule in the training set respectively, is the average activity of all the molecules in the training set. However, the external validation was computed from the test compounds (q^2) using the equation:

$$\frac{\Sigma}{\Sigma}$$ Eq.3

where and are the predicted and actual activities of the *i*th molecule in the test set respectively, is the average activity of all the molecules in the training set.

In addition, the model was also evaluated for survival score, adjusted survival scores, Pearson-R coefficient and F distribution values. Furthermore, the test set was externally validated [56-58] for various essential parameters like ,
and k value using XternalValidationPlus 1.0 [59] by employing the following equations:

$$\sqrt{\quad}$$ Eq.4

$$\frac{\Sigma}{\Sigma}$$ Eq.5

Where, is the average of the predicted value of compounds in the dataset. The regression of against through the origin should have *k* nearer to 1 and the slope can be calculated using Equation 6.

Eq.6

2.1.5. Applicability Domain Study (AD)

QSAR applicability domain study was performed to analyse the significance of the model for reliable predictions [60]. It represents structural or biological space and physicochemical knowledge information based on the training set of the model that is used for the prediction of test compounds. Moreover, it also specifies the scope of the proposed model and defines model limitations with respect to structural domain [61]. Using this method, compounds beyond the scope of model can be delineated and retracted from the training set. Further investigation of the dataset was employed by mathematical means for the biological conception that model compounds should possess structural correlation in regard to active site in which they fit. Here, we have used the algorithm and methodology proposed by Roy *et al*. to define training set outliers and recognition for the compounds existing outside the AD [62, 63].

2.1.6. Virtual Screening

Virtual screening was performed to retrieve hits from ZINC natural products database (84215 compounds) using the pharmacophore model [64, 65]. The IBScreen NP database was downloaded (http://zinc.docking.org/) in .mol2 format and prepared for fixing suitable geometries using *Ligprep* wizard. Subsequently, *advanced pharmacophore screening* workflow of PHASE was used to map and rank the database compounds on the selected hypothesis. Per rotatable bond 10 and maximum of 200 conformers of each library compounds were generated, within a relative energy window of 10.0 kcal/mol. To gauze the best mapping and

realistic outcomes, *thorough* mode of ligand sampling was used.

2.1.7. Molecular Docking

Screened *hits* obtained from ligand-based method (pharmacophore) were further studied for structure-based studies (docking) using LeadIt 2.1.8 [35]. The program uses FlexX approach and considers ligand flexibility with changing ligand conformations. It uses incrementally build up algorithm and starts docking with base fragment [66]. However, after placing the base fragment, whole ligand is built up by adding remaining fragments on to it. The protocol purely considers protein as rigid.

The study was planned to investigate the intermolecular interactions between the *hits* (ligands) and the target *i.e.*, *Vinca* binding domain of the tubulin protein. The X-ray crystal structure of stathmin like-domain complex (RB3-SLD) [PDB entry code: 1Z2B] was retrieved from the Protein Data Bank (http://www.rcsb.org) [67, 68]. Prior to docking, ligands were pre-processed using *prepare ligand* wizard in Accelrys *Discovery Studio 4.0*. The active site of receptor was defined in LeadIT considering a radius 10 Å (from the centroid of the co-crystallised ligand *i.e.*, vinblastine). The method uses empirical scoring function (LeadIT score) which computes the binding energy (ΔG) of the ligand-protein complex by following equation.

$$= \quad \times = + \qquad + \qquad {}_{lipocount} + * (R, \Delta\alpha)$$

Here, $+ * (R, \Delta\alpha)$ is a scaling function penalizing deviation from ideal geometry. is the number of free rotatable bonds that are confined in the complex [69]. The terms ΔG_o and ΔG_{lipo} are adjustable parameter and lipophilic contact energy respectively. Finally, the poses containing the highest score were selected for analysing the ligand-receptor interactions.

2.1.8. Molecular Dynamics (MD) Studies

MD simulations were performed by using Desmond version 2.0 (Academic Version) [70-72] which utilises neural territory method for exploiting greater degree of computational parallelism [73]. The highest scored retrieved *hits* from virtual screening and docking were examined by MD for over a period of 10ns. OPLS-2005 force field parameterizations [37] were used to model interactions and conformational behavior in a solvation system of SPC (Simple Point Charge) water molecules as solvent [34]. The solvation system was constructed with orthorhombic boundary condition (10 Å × 10 Å × 10 Å) ensuring that the whole complex covered. Thereafter, the system was neutralised by adding 87 sodium ions (73.175 mM) and 60 chloride ions (50.465 mM) to balance the net charge of the system. Prior to MD, the solvated system (comprise of 77819 atoms) was allowed to pre-equilibrate using default relaxation parameters in a series of restrained steps as implemented in Desmond.

The electrostatic interactions were treated by particle-mesh Ewald method for long range whereas cut-off of 9Å was used for short range van der Waals and coulombic interactions [74]. Further, Isothermal-Isobaric NPT ensemble was used with the temperature of 300K (Nose-Hoover thermostat) and 1bar pressure [75]. Subsequently, the MD trajectory was recorded at an interval of every 10ps for over a period of 10ns to capture 1000 MD frames. The structural changes and dynamic behaviour of the protein were analyzed by calculating the RMSD and energy.

3. RESULTS AND DISCUSSION

Rationale behind this work was to cognise the structural features and pharmacophoric requirements critical for the ligand binding at *Vinca* site of the tubulin. Furthermore, to identify the novel compounds using the pharmacophore based virtual screening.

3.1. Pharmacophore Modelling

The reported modelling work employs PHASE 3D-QSAR formalism that has various advantages over to other older approaches. Particularly, it applies tree-based partitioning algorithm to generate bit string representations of the ligands and bi-directional clustering approach to distinguish multiple binding modes [76]. Several six, five and four-point pharmacophore hypotheses were generated using six actives (>5.769) and five inactives (<4.958). The selected ligand molecules (actives/inactives) were used to test and generate the hypotheses and for defining the excluded volumes of inactives [77]. The remaining molecules of the dataset were used to further validate and authenticate the pharmacophore model.

All the possible hypotheses from the set of actives and identical sets of features with similar spatial arrangement were congregated to recognize a common pharmacophore. Subsequently, a list of 71 combinations of site feature variants were obtained as possible Common Pharmacophore Hypotheses (CPH) having at least five site features that must match on four active molecules. These variant combinations were scored by active and inactive compounds to identify a set of hypotheses to extract best alignment of all chosen actives. The three and four featured CPHs were rejected as they were unable to define the complete binding space and regression contours. Overall, 326 possible CPHs were generated and subjected for rigorous scoring analysis for site, vector, and volume. In scoring, biological activity of compounds (pIC50) was included in the score with a weight of 1.0, however reference relative conformational energy (kJ/mol) was incorporated with a weight of 0.01. The resulting hypotheses were scored with respect to the fixed actives and inactives. The summary of the hypotheses survived with their survival scores are listed in Table **2**. The hypothesis AADDH.5352 was selected due to its superiority of scores and ability to distinguish from actives and inactives. The hypothesis was represented with two donor features (D), two acceptor features (A) and one hydrophobic feature (H) (Fig. **2**). Feature representations with inter-feature distances (depicted in Fig. **2a**) and inter-feature angles (Table **S3**, †ESI) were the principal attribute that distinguished active from inactives.

Larger value of the survival- inactive score *i.e.*, 2.127 indicate that the hypothesis can successfully discriminates actives and inactives substantially. The greater value of Post-Hoc score for this hypothesis (2.65) specifies that the model

Table 2. Score of different hypothesis generated in pharmacophore building.

ID	Survival	Survival - Inactive	Post-hoc	Site	Vector	Volume	Energy
AADDH.5352**	2.864	2.127	2.654	0.5	0.806	0.34	8.82
ADHHP.169	2.857	1.482	2.647	0.46	0.948	0.23	14.70
ADHHP.153	2.854	1.674	2.645	0.46	0.947	0.24	16.51
ADHHP.168	2.853	1.439	2.643	0.46	0.945	0.24	2.96
ADHHP.172	2.847	1.439	2.637	0.45	0.944	0.24	8.89
ADHHP.154	2.838	1.396	2.628	0.44	0.942	0.24	7.02
ADHHP.170	2.829	1.66	2.619	0.44	0.941	0.24	20.39
ADHHP.2	2.827	1.393	2.617	0.43	0.935	0.25	24.91
ADHHP.171	2.821	1.626	2.611	0.43	0.938	0.24	16.50

** Selected hypothesis used for modelling studies

was highly reliable. Moreover, the Site and Vector Score values (0.50 and 0.80 respectively) further endorse that the site points and corresponding functionalities were superimposed well. The mapping of AADDH.5352 over to the highest active compound in Fig. (**2b**) further insinuates that most of the features completely overlap onto the ligand functionalities. Conversely, mapping on the most inactive molecule in Fig. (**2c**) was unable to overlay on most of the ligand functionalities. This observation led to the conclusion that selected pharmacophore model can distinguish inactive ligands from the set of actives. It can be anticipated that chemical structure posing these feature with the given stereo-electronic requirement and at the cited region in particular, would probably adjusts systematic structure-activity relationships for tubulin inhibition activity [78]. Therefore, screening with Virtual and high throughput methods using pharmacophore can lead to the identification of potent, efficacious and orally bioavailable analogues [79]. In addition, the presence and absence of such groups can be quantified by building the QSAR model that can be used to screen the matches in the database as well as identification of the functional groups contributing negatively or positively to activity.

3.2. 3D-QSAR Modelling

On the way to correlate the biological activity as dependent variable with the binary value (ligand descriptors) as independent variable, atom based 3D-QSAR model was generated using the four factor PLS [80]. Increase in PLS components beyond four did not improve the statistics or predictive ability of the model [81]. The best model was selected corresponding to second PLS factor with hypothesis AADDH.5352 on the basis of relatively high value of cross validation coefficient *i.e.*, 0.729 and low RMSE. QSAR analysis shows that the selected pharmacophore hypothesis display good correlation with statistically significant values of = 0.986 and standard deviation (SD) 0.206. Moreover, significance of model was further supported by meaningful RMSE 0.110, Pearson-R 0.879 and *F*-statistics value 562.9 (Table **3**). As shown in Table **3**, the statistics lies in good agreement with large value of *F* and small value of *P*; an indication of a high degree of confidence. The selected best model was further validated for their external predictive reliability using Pearson coefficient of correlation (Pearson-R) which was found to be 0.879.

Further, the goodness and model predictability was analyzed by and metrics as depicted in Table **4**. The correlation plots between the predicted activity of training set molecules exhibits satisfactory linear correlation with minor differences in experimental/predicted activities (Fig. **S2**, Table **S1**).

3.3. QSAR Contour Plot Analysis

PHASE renders the additional insights into structure-activity relationship (SAR) by visualizing the effects due to respective pharmacophoric feature and their associated positive and negative regression coefficients. The visualization was performed by contour plots to perceive and recognize the discrete vital pharmacophoric requirements at spatial sites of structure. Moreover, these maps identify the presence and absence of essential chemical feature. Nonetheless, this allow identification of those positions that require a particular physicochemical property to enhance bioactivity of a ligand [82]. The contour plots represent positive and negative activity coefficients of (a) hydrogen bond donor, (b) electron withdrawing property, (c) hydrophobic/non-polar and (d) negative ionisable properties. Positive and negative contributions are depicted by blue cubes and red cubes respectively. Further, owing to high structural diversity, it was quite difficult to display the pharmacophore model on all ligands or the subsets of ligands. Therefore, we have depicted the contour plot of most active ligand *i.e.*, diazonamide (Fig. **3**) for better understanding of the groups substitution effects. Moreover, it can illustrate the spatial site points where a particular functionality directs the activity. In Fig. (**3a**) for H-bond donor, blue contour situated at –OH group (D11) and –NH functionality nearby 1,3 oxazole ring whereas it was unfavourable around dimethyl group. Fig. (**3b**) displays contour map for hydrophobic property and the blue contours mainly located near to the bridged carbon, on chloro group

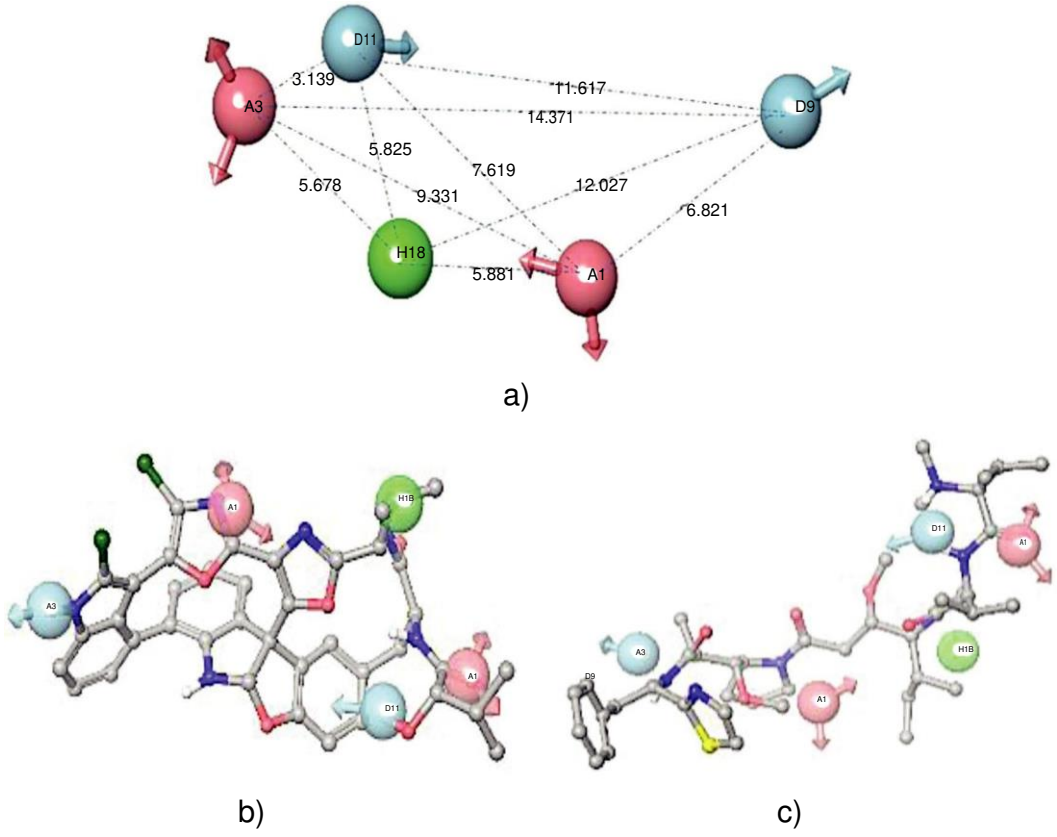

Fig. (2). Stereoviews of the best pharmacophore model**: a**) Common pharmacophoric site features with inter-site distances between the pharmacophoric points (All distances are in Å unit), **b**) mapping of AADDH.5352over the highest active molecule, and **c**) mapping of AADDH.5352over the highest inactive molecule.

Table 3. PLS statistical parameters of the selected 3D-QSAR model.

ID	# Factors	SD	r^2	F	P	RMSE	q^2	Pearson-R
AADDH-5352	1	0.206	0.867	111.4	6.98E-09	0.135	0.56	0.86
	2	0.069	0.986	562.9	1.49E-15	0.11	0.729	0.879
	3	0.024	0.998	3042.7	4.20E-21	0.104	0.76	0.897
	4	0.008	0.999	17851	8.90E-26	0.104	0.758	0.906

SD, standard deviation of regression; r^2 is for the regression coefficient; **F** is the ratio of the model variance to the observed activity variance (variance ratio); **P**, significance level of variance ratio.; **RMSE**, root-mean-square error, directly analogous to but based on the test set predictions or it can be better referred as $R^2_{pred,}$ **Pearson R** value for the correlation between the predicted and observed activity for the test set; RMSE the RMS error in the test set predictions.

and at the centre of the bulkier rings. The effect of positive ionic group demonstrates (Fig. **3c**) that such groups were not required in between carbonyl of amide and dimethyl groups. Furthermore, Fig. (**3d**) depicts the contour map for electron withdrawing property that describes the favourable blue contours were demanded near to the oxygen of furan ring and –NH of amide group whereas opposed at chloro substitution position.

Table 4. External validation parameters for the QSAR model.

		| - |	k
0.98583	0.9846	0.00017	0.99974

Model acceptable criteria: >0.5; >0.5; | - |<0.3) and $0.85 \leq k \geq 1.15$

3.4. Applicability Domain (AD) Study

The study was conducted by standardization approach [63] to find compounds that resides outside the AD. The result shows that there were no any X-outliers in training and test set which eliminate the chances of uncertainty associated with the predictions. This also substantiates that training set compounds possess some functional correlation in terms of structure and their modelled 3D descriptors and modelled response resides within the AD.

3.5. Virtual Screening and ADME Properties Calculation

Ligand based virtual screening [83] was executed utilizing the AADDH.5352 hypothesis as query to screen ZINC Natural product (NP) database to identify compounds

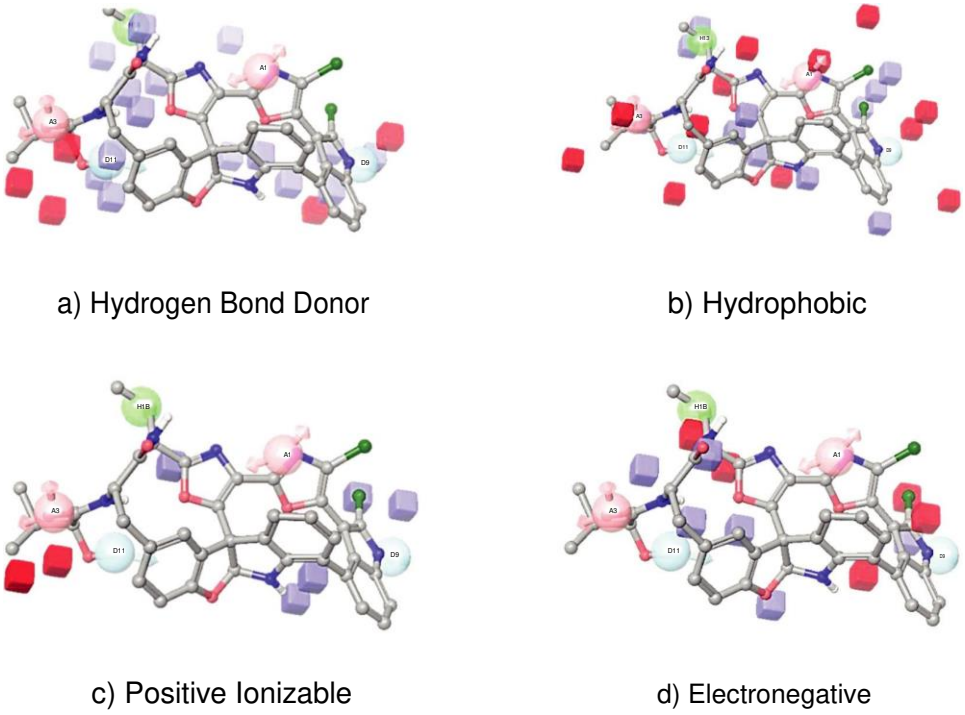

Fig. (3). Contour maps for 3D-QSAR models generated for most active *Vinca* binders *i.e*., Diazonamide A: hydrogen bond donor (**a**), hydrophobic (**b**), positive ionic (**c**) and electron withdrawing property (**d**) Blue contours correspond to the regions where the substitution of corresponding property group enhances the activity and vice versa for the red contours (Color illustration is available online).

with similar physical and chemical properties (pharmacophore-based, descriptor-based) and likely to interact with the target [55]. Screening with the defaults parameters retrieved 596 molecules as *hits* that encompass the maximum fitness of 1.320 to 1.195 with four minimum number of site feature mapping threshold. Here, we majorly focussed on apprehending novel scaffolds inspired from diverse NP chemical functionalities. Nevertheless, these can be used as a guiding functionalities for the synthesis of promising new compounds. Overall, there were significant correlation between the fitness scores and tubulin binding activities of the compounds. Furthermore, receptor based virtual screening (docking) approach was also used to examine selectivity and for narrowing down the ligand-based screening results. Prior to docking studies, all the *hits* were examined for their ADME/T attributes.

The ADME/T properties of the molecules are an essential guide for lead generation that avoids the failure of candidates in later stages attritions due to their poor pharmacokinetic profile [84]. The so called *'drug likeness'* was estimated by calculating various ADME parameters using *'QikProp'* program of Schrödinger Software [85] (Table **S3**).

From 596 ligands, 559 compounds passed the ADME filters that follows Lipinski rule of five [86] and Verber rule of three [87].

Conspicuously, analysis of therapeutically relevant descriptor like QPlogPo/w, QPlogS, QPPCaco, QPlogBB, QPlogMDCK and polar surface area (PSA) also lies in the regimen of biological relevance.

3.6. Molecular Docking

Molecular docking study was performed using FlexX approach to study the ligand-receptor binding pattern [55]. The screened *hits* were analysed for interfering the tubulin assembly at *Vinca* domain located around RB3 stathmin peptide (RB3-SLD) [PDB entry code: 1Z2B] [67, 88, 89]. Moreover, the description of binding site was also taken from PDBsum [90] (Fig. **S3**). Based on >1.180 fitness score, 99 ligands were used for docking among all the ADME filtered *hits*. The docked poses of the ligands that dominate in energetics and favorable interactions were analyzed, and found that ligands were adequately bound in the pocket with significant energy ranging from -30.298 to -11.778 kJ/mol. Scoring results for best fit twenty ligands in the binding pocket are tabulated in the Table **5**. Simplifying the docking results for the docked poses of the compounds, we have chosen highest scored four representative ligands. Visualizations of the interacting amino acids with the ligands are depicted in Fig. (**4**). It was observed that the binding site and interacting amino acids were located in between chain B and C of tubulin protein. Intriguingly, most of the reference functionalities (present in co-crystallised structures) were found to associate with the docked screened *hits*. Depiction of the interaction maps and details of non-covalent interaction types are represented in ESI (Fig. **S4** and Fig. **S5**, †ESI). Furthermore, structural alignment of *hits* in active domain of tubulin were also compared and contrasted as displayed in Fig. (**5**). Superimposition of screened *hits* on to the reference ligands illustrates that ligands own functional correlation and aligns very similar over to the known crystallized ligand.

Table 5. 20 Best docked compounds enumerated after LeadIt docking with their scores.

Name	E_Total	E_Match	E_Lipo	E_Clash	ΔG
ZINC72325117	-29.106	-26.429	-9.342	2.99	-23
ZINC59489217	-30.298	-31.753	-9.692	7.734	5
ZINC08764417	-25.53	-27.347	-7.419	4.584	-2
ZINC12893948	-25.45	-28.021	-10.096	8.36	-20
ZINC02113067	-25.029	-32.885	-7.2	8.175	12
ZINC32123863	-24.962	-26.037	-12.198	5.737	-15
ZINC04029355	-24.548	-34.471	-4.32	3.345	-11
ZINC12664540	-24.122	-21.634	-9.414	6.013	19
ZINC02120497	-23.868	-24.544	-10.353	3.128	-1
ZINC02134676	-23.794	-28.709	-9.411	4.913	5
ZINC02112420	-23.349	-24.196	-8.788	4.799	16
ZINC96221829	-23.289	-25.388	-7.317	1.909	17
ZINC72325903	-22.968	-21.26	-10.967	3.985	-6
ZINC06623887	-22.949	-29.04	-7.623	2.811	-10
ZINC02140391	-22.776	-28.052	-7.229	3.611	2
ZINC32124152	-22.767	-27.824	-5.663	4.13	-8
ZINC08879023	-22.721	-22.474	-12.83	3.422	-12
ZINC09033913	-22.699	-24.288	-9.504	9.968	8
ZINC70672753	-22.388	-19.229	-14.175	6.462	-1
ZINC96115293	-22.332	-27.017	-7.912	2.215	8

****Total Score (E_TOTAL),** Total score of the docking solution; **Match Score (E_MATCH),** Contribution of the matched interacting groups; **Lipo Score (E_LIPO),** Contribution of the lipophilic contact area; **Ambig Score (E_AMBIG),** Contribution of the lipophilic–hydrophilic (ambiguous) contact area; **Clash Score (E_CLASH)**, Contribution of the clash penalty; ; **Avg. Volume (AVG_VOL),** Average volume of protein/ligand overlap (for a description of the overlap test; **Max Volume (MAX_VOL),** Maximum volume of protein/ligand overlap (for a description of the overlap test and **ΔG,** Binding Free energy(kJ/mol) .

Ligand ZINC72325117 shows hydrogen bond with Ala247 C, Tyr224 B, Asn329 C, Asn249 C and significant Van der Waals interactions with the Thr223 B, Val353 C, Val177 B, Gly354 C, Pro222 B, Ileu 355 C and Gly225 B residues. The total docking score was -29.106 kJ/mol with E_Match, E_Lipo and E_Clash score as -26.42, -9.342 and 2.99 respectively. However, ligand ZINC59489217 possesses the total docking energy -30.298 kJ/mol with lipophilic and matching scores of -9.62 and -31.75 kJ/mol respectively. Among bonding interactions, H-bonding was formed with amino acids Asp179 and Tyr224 in B chain whereas Asn249 and Val177 residues in C chain. This comprehends that ligand fits adequately in the binding pocket and would anticipates greater biological activity. Beyond the activity, specificity and sensitivity of screened obtained ligands were also taken into consideration in order to prioritize the ligands as suggested by Chopra *et al.* [91].

Furthermore, Gibbs free energy of binding () were also computed by HYDE assessment [92] for gauzing atom based hydration and desolvation effects of ligand-receptor

(Eq. 3)

Compound ZINC72325117 possess significant ΔG score, -23.0kJ/mol which implies that it can exhibits substantial H-bonding and weak desolvation energies. Further, greater negative scores indicate weak desolvation penalties and compound can easily ligated with the *Vinca* domain through bonding interactions (ZINC12893948, ZINC32123863). In contrary, ligands that were solvated strongly and form imperfect hydrogen bond of deviated length were able to secured positivevalues.

3.7. Molecular Dynamics Studies

To understand the structural integrity and for observing the interactions along the dynamic behaviour of the protein-ligand complex, the MD simulations were executed with the highest ranked hit molecule ZINC72325117. In addition, this was performed to examine the ligands dynamical behavior and overall thermodynamic stability of the proposed *hit* molecule. The RMSD values of the modelled protein as well as ligand backbone atoms is plotted as a time-dependent function in Fig. (**6a**). It is imperative from the results that there was constant RMSD deviation throughout the whole simulation run. In particular, fluctuations in the protein RMSD was broadly ranged from 1.0 to 1.75A, however ligand RMSD was deviated from 0.3 to 2.3Å. The only significant deviation was captured in between the time interval of 5 to 6ns. Overall, low RMSD indicate that the protein-ligand complex represents a stable entity and symbolizes for the possible tubulin inhibitor. The graph of the ligand RMSF, protein per residue contacts and change in various molecular properties are depicted in supplementary information.

Further, the trajectory was post-processed for investigating the key information of protein binding using "*simulation-interaction diagram"* implemented in the Maestro interface. Interaction types were grouped into four subtypes: hydrogen-bond, hydrophobic interactions, ionic bonds and water bridges. The results were profiled in the stacked bar plots in the Fig. (**6c**). The Fig. (**6d**) clearly deciphers that OH and carbonyl oxygen of quinazoline ring and NH of amide linker engaged in developing the non-covalent interactions on the ligand. However, from the protein active site residues Val177B, Ser178B and Asn101B interaction remain intact for almost 77%, 31% and 41% of the total simulation time. Importantly, water-bridge interactions were observed in between the OH of the quinazoline and Asn101 of the vinca domain of tubulin protein (Fig. **6c**).

4. DISCUSSION ON SCREENED HITS

In the present scenario of ever increasing pressure on the pharma industry to accelerate its drug discovery process, current state-of-the-art computational methods seem to stipulate the goals [94, 95]. In particular, the *hits* retrieved in the present study are difficult to contemplate by conventional methods. Owing to this, we envisage the dominating chemical functionalities involved in the ligand-receptor binding event of the tubulin protein. The proposed *hits* (Fig.

complex [93], by employing Equation 3.

S6) were reported to comprise essential features and

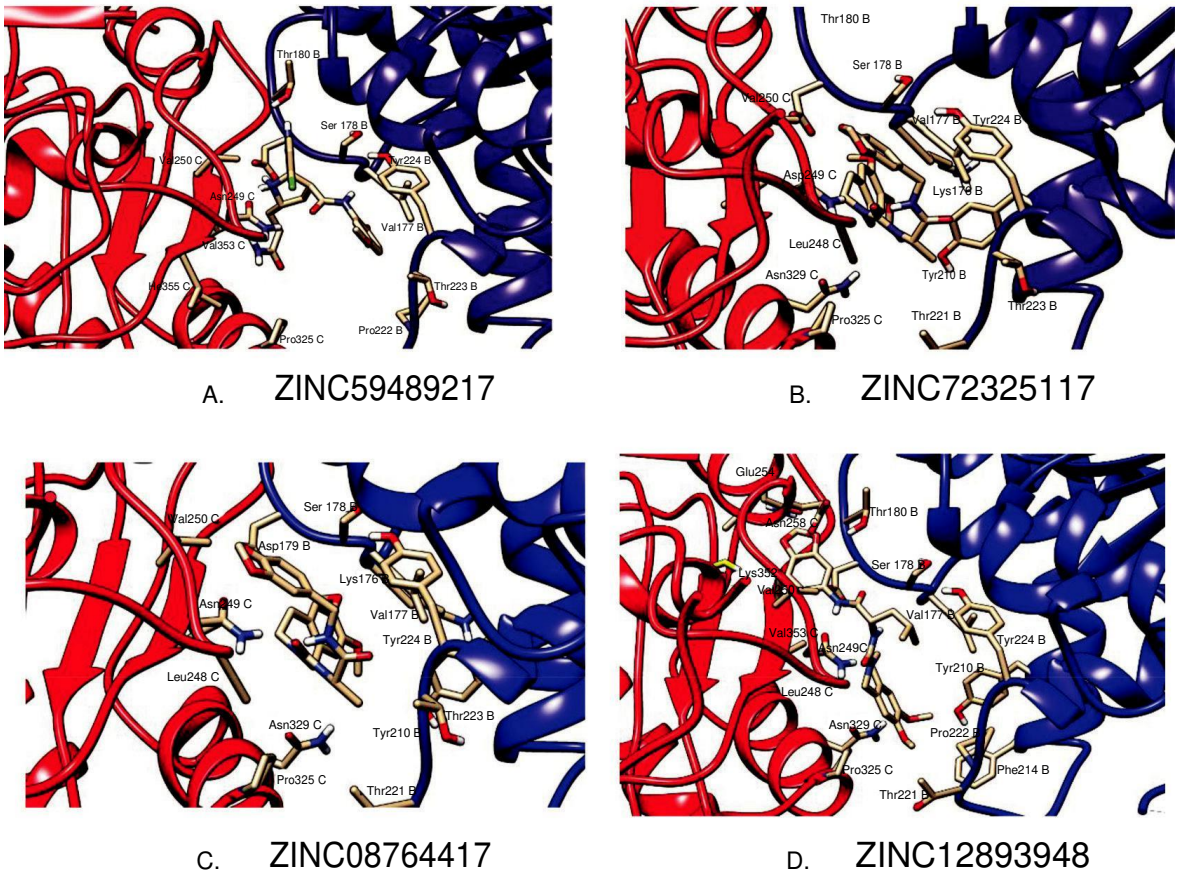

Fig. (4). Docking poses and their interactions with the residue present in the active site of the protein (generated from visualizer, UCSF Chimera).

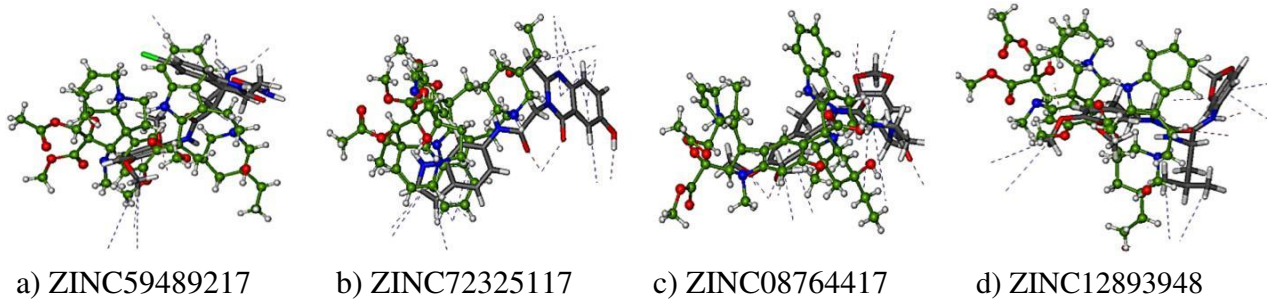

Fig. (5). Overlay of the reference ligand *i.e.*, vinblastine (in green colour) over to the docked ligand inside the binding pocket of the tubulin protein (Color illustration is available online).

orient in the binding site similar to the reference compounds. We anticipate that despite of comprising different structures or functional features, the *hits* possess healthy correlation in terms of biological potentials. Moreover, the presence of similar ligand-receptor interaction [67] minimizes the ambiguities associated with pharmacophore based virtual screening.

CONCLUSION

Structure-activity insight was rendered into the vinca domain of tubulin by the computational studies. The quantitative pharmacophore model was developed from the range of known active natural product scaffolds to incorporate essential complimentary features accountable for inhibition. The hypothesis meets the model acceptable criteria as observed from atom-based QSAR and applicability domain studies. Hence, the constructed model was subsequently employed for screening the diversified natural product database to uncover the analogs with improved potencies. We reported that the retrieved *hits* mimicked the binding pattern and orientation of the experimental pose. Through these results, it can be said that the hierarchical combination of methods can associatively steer the identification of novel scaffolds. The approach in principle proves the efficiency of the method and offer rationales for further lead optimization.

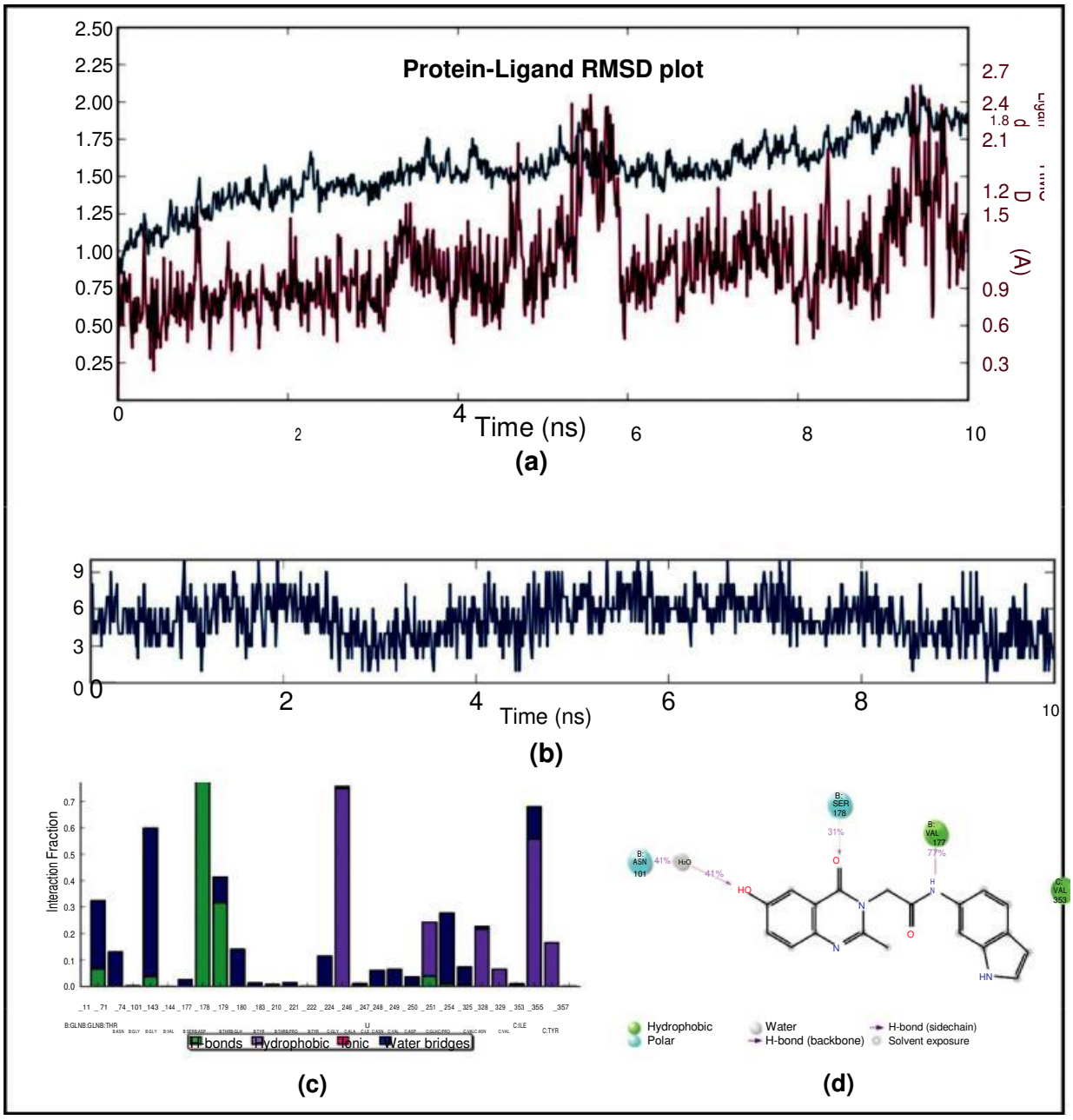

Fig. (6). Protein-Ligand RMSD and Contacts between the active site amino acids and the ligands during the course of 10ns MD simulation (**a**) Protein-Ligand RMSD plot (**b**) Number of total contacts; (**c**) Ligand atom percentage contribution with the protein residues; and (**d**) Interaction type of the protein residue contributing to the interaction.

CONSENT FOR PUBLICATION

Not applicable.

CONFLICT OF INTEREST

The authors declare no conflict of interest, financial or otherwise.

ACKNOWLEDGEMENTS

This work was supported by Department of Science & Technology (DST), New Delhi under INSPIRE-JRF grant awarded to Mohd. Athar. Ashish K. Radadiya is thankful to the University Grants Commission (UGC, New Delhi) for UGC-BSR fellowship. Prakash C. Jha would also like to thank UGC for start-up grant. The authors also acknowledge Central University of Gujarat-Gandhinagar (CUG) and Center of Excellence, National Facility for Drug Discovery Complex, Saurashtra University-Rajkot (COE-NFDD) for providing basic infrastructure and facilities.

SUPPLEMENTARY MATERIAL

Supplementary material is available on the publisher's website along with the published article.

REFERENCES

[1] Jordan, M. Mechanism of action of antitumor drugs that interact with microtubules and tubulin. *Curr. Med. Chem. Anti-Cancer Agents,* **2002**, *2*(1), 1-17.

[2] Nogales, E. Structural insights into microtubule function. *Ann. Rev. Biochem.,* **2000**, *69*(1), 277-302.

[3] Perez, E.A. Microtubule inhibitors: Differentiating tubulin-inhibiting agents based on mechanisms of action, clinical activity, and resistance. *Mol. Cancer Ther.,* **2009**, *8*(8), 2086-2095.

[4] Vindya, N.; Sharma, N.; Yadav, M.; Ethiraj, K. Tubulins-the target for anticancer therapy. *Curr. Topics Med. Chem.,* **2015**, *15*(1), 73-82.

[5] Jain, A.N. Virtual screening in lead discovery and optimization. *Curr. Opin. Drug Discov. Devel.,* **2004**, *7*(4), 396-403.

[6] Jordan, M.A.; Wilson, L. Microtubules as a target for anticancer drugs. *Nat. Rev. Cancer,* **2004**, *4*(4), 253-265.

[7] Li, Q.; Sham, H.L. Discovery and development of antimitotic agents that inhibit tubulin polymerisation for the treatment of cancer. *Expert Opin. Therapeut. Patents,* **2002**, *12*(11), 1663-1702.

[8] Prinz, H. Recent advances in the field of tubulin polymerization inhibitors. *Expert Rev. Anticancer Ther.,* **2002**, *2*(6), 695-708.

[9] Beckers, T.; Mahboobi, S. Natural, semisynthetic and synthetic microtubule inhibitors for cancer therapy. *Drugs Future,* **2003**, *28*(8), 767-785.

[10] Nogales, E.; Wolf, S.G.; Downing, K.H. Structure of the alpha beta tubulin dimer by electron crystallography. *Nature,* **1998**, *391*(6663), 199-203.

[11] Pellegrini, F.; Budman, D.R. Review: tubulin function, action of antitubulin drugs, and new drug development. *Cancer Invest.,* **2005**, *23*(3), 264-273.

[12] Islam, M.; Iskander, M.N. Microtubulin binding sites as target for developing anticancer agents. *Mini Rev. Med. Chem.,* **2004**, *4*(10), 1077-1104.

[13] Gupta, S.; Bhattacharyya, B. Antimicrotubular drugs binding to vinca domain of tubulin. *Mol. Cell Biochem.,* **2003**, *253*(1-2), 41-47.

[14] Jordan, M.A.; Wendell, K.; Gardiner, S.; Derry, W.B.; Copp, H.; Wilson, L. Mitotic block induced in HeLa cells by low concentrations of paclitaxel (Taxol) results in abnormal mitotic exit and apoptotic cell death. *Cancer Res.,* **1996**, *56*(4), 816-825.

[15] Lee, K.-H. Discovery and development of natural product-derived chemotherapeutic agents based on a medicinal chemistry approach †. *J. Nat. Prod.,* **2010**, *73*(3), 500-516.

[16] Cassady, J.M.; Baird, W.M.; Chang, C.-J. Natural products as a source of potential cancer chemotherapeutic and chemopreventive agents. *J. Nat. Prod.,* **1990**, *53*(1), 23-41.

[17] Cragg, G.M.; Newman, D.J.; Snader, K.M. Natural products in drug discovery and development. *J. Nat. Prod.,* **1997**, *60*(1), 52-60.

[18] Mukhtar, E.; Adhami, V.M.; Mukhtar, H. Targeting microtubules by natural agents for cancer therapy. *Mol. Cancer Therapeut.,* **2014**, *13*(2), 275-284.

[19] Lu, Y.; Chen, J.; Xiao, M.; Li, W.; Miller, D.D. An overview of tubulin inhibitors that interact with the colchicine binding site. *Pharmaceut. Res.,* **2012**, *29*(11), 2943-2971.

[20] Chen, S.M.; Meng, L.H.; Ding, J. New microtubule-inhibiting anticancer agents. *Expert Opin. Investig. Drugs,* **2010**, *19*(3), 329-343.

[21] Silvestri, R.; New prospects for vinblastine analogues and anticancer agents. *J. Med. Chem.*, **2013**, *2013*, 625-627.

[22] Bai, R.; Pettit, G.R.; Hamel, E. Binding of dolastatin 10 to tubulin at a distinct site for peptide antimitotic agents near the exchangeable nucleotide and vinca alkaloid sites. *J. Biol. Chem.,* **1990**, *265*(28), 17141-17149.

[23] Johnson, I.S.; Armstrong, J.G.; Gorman, M.; Burnett, J.P. Jr. The Vinca Alkaloids: A New Class of Oncolytic Agents. *Cancer Res.,* **1963**, *23*(8 Part 1), 1390-1427.

[24] Thrower, D.; Jordan, M.A.; Wilson, L. Quantitation of cellular tubulin in microtubules and tubulin pools by a competitive ELISA. *J. Immunol. Methods,* **1991**, *136*(1), 45-51.

[25] Manetti, F.; Maccari, L.; Corelli, F.; Botta, M. 3D QSAR models of interactions between β-tubulin and microtubule stabilizing antimitotic agents (MSAA): A survey on taxanes and epothilones. *Curr. Top. Med. Chem.,* **2004**, *4*(2), 203-217.

[26] Kandakatla, N.; Ramakrishnan, G.; Karthikeyan, J.; Chekkara, R. Pharmacophore Modeling, Atom based 3D-QSAR and docking studies of chalcone derivatives as tubulin Inhibitors. *Oriental J. Chem.,* **2014**, *30*(3), 1083-1098.

[27] ter Haar, E.; Rosenkranz, H.S.; Hamel, E.; Day, B.W. Computational and molecular modeling evaluation of the structural basis for tubulin polymerization inhibition by colchicine site agents. *Bioorg. Med. Chem.,* **1996**, *4*(10), 1659-1671.

[28] Salum, L.B.; Dias, L.C.; Andricopulo, A.D. Structural and chemical basis for anticancer activity of a series of²-tubulin ligands: molecular modeling and 3D QSAR studies. *J. Brazilian Chem. Soc.,* **2009**, *20*(4), 693-703.

[29] Drewry, D.H.; Macarron, R. Enhancements of screening collections to address areas of unmet medical need: an industry perspective. *Curr. Opin. Chem. Biol.,* **2010**, *14*(3), 289-298.

[30] Harvey, A.L.; Edrada-Ebel, R.; Quinn, R.J. The re-emergence of natural products for drug discovery in the genomics era. *Nat. Rev. Drug Discov.,* **2015**, *14*(2), 111-129.

[31] Dumontet, C.; Jordan, M.A. Microtubule-binding agents: a dynamic field of cancer therapeutics. *Nat. Rev. Drug Discov.,* **2010**, *9*(10), 790-803.

[32] Dixon, S.L.; Smondyrev, A.M.; Knoll, E.H.; Rao, S.N.; Shaw, D.E.; Friesner, R.A. PHASE: a new engine for pharmacophore perception, 3D QSAR model development, and 3D database screening: 1. Methodology and preliminary results. *J. Comput. Aided Mol. Des.,* **2006**, *20*(10-11), 647-671.

[33] Dixon, S.L.; Smondyrev, A.M.; Rao, S.N. PHASE: a novel approach to pharmacophore modeling and 3D database searching. *Chem. Biol. Drug Des.,* **2006**, *67*(5), 370-372.

[34] Kaminski, G.A.; Friesner, R.A.; Tirado-Rives, J.; Jorgensen, W.L. Evaluation and reparametrization of the OPLS-AA force field for proteins *via* comparison with accurate quantum chemical calculations on peptides. *J. Phys. Chem. B,* **2001**, *105*(28), 6474-6487.

[35] LeadIt *BioSolveIT GmbH*, 2.1.8; Sankt Augustin Germany.

[36] LigPrep Schrödinger Release 2014-4, Schrödinger, LLC, New York, NY: 2014.

[37] Jorgensen, W.L.; Maxwell, D.S.; Tirado-Rives, J. Development and testing of the OPLS all-atom force field on conformational energetics and properties of organic liquids. *J. Am. Chem. Soc.,* **1996**, *118*(45), 11225-11236.

[38] Watts, K.S.; Dalal, P.; Murphy, R.B.; Sherman, W.; Friesner, R.A.; Shelley, J.C. ConfGen: a conformational search method for efficient generation of bioactive conformers. *J. Chem. Inf. Model.,* **2010**, *50*(4), 534-546.

[39] Hill, B.T. Vinflunine, a second generation novel Vinca Alkaloid with a distinctive pharmacological profile, now in clinical development and prospects for future mitotic blockers. *Curr. Pharm. Des.,* **2001**, *7*(13), 1199-1212.

[40] Bai, R.L.; Pettit, G.R.; Hamel, E. Structure-activity studies with chiral isomers and with segments of the antimitotic marine peptide dolastatin 10. *Biochem. Pharmacol.,* **1990**, *40*(8), 1859-1864.

[41] Towle, M.J.; Salvato, K.A.; Budrow, J.; Wels, B.F.; Kuznetsov, G.; Aalfs, K.K.; Welsh, S.; Zheng, W.; Seletsky, B.M.; Palme, M.H.; Habgood, G.J.; Singer, L.A.; Dipietro, L.V.; Wang, Y.; Chen, J.J.; Quincy, D.A.; Davis, A.; Yoshimatsu, K.; Kishi, Y.; Yu, M.J.; Littlefield, B.A. *In vitro* and *in vivo* anticancer activities of synthetic macrocyclic ketone analogues of halichondrin B. *Cancer Res.,* **2001**, *61*(3), 1013-1021.

[42] Smith, J.A.; Wilson, L.; Azarenko, O.; Zhu, X.; Lewis, B.M.; Littlefield, B.A.; Jordan, M.A. Eribulin binds at microtubule ends to a single site on tubulin to suppress dynamic instability. *Biochemistry,* **2010**, *49*(6), 1331-1337.

[43] Kuznetsov, G.; TenDyke, K.; Towle, M.J.; Cheng, H.; Liu, J.; Marsh, J.P.; Schiller, S.E.; Spyvee, M.R.; Yang, H.; Seletsky, B.M.; Shaffer, C.J.; Marceau, V.; Yao, Y.; Suh, E.M.; Campagna, S.; Fang, F.G.; Kowalczyk, J.J.; Littlefield, B.A. Tubulin-based antimitotic mechanism of E7974, a novel analogue of the marine sponge natural product hemiasterlin. *Mol. Cancer Ther.,* **2009**, *8*(10), 2852-2860.

[44] Kobayashi, M.; Natsume, T.; Tamaoki, S.; Watanabe, J.i.; Asano, H.; Mikami, T.; Miyasaka, K.; Miyazaki, K.; Gondo, M.; Sakakibara, K. Antitumor activity of TZT-1027, a novel doiastatin 10 derivative. *Jpn. J. Cancer Res.,* **1997**, *88*(3), 316-327.

[45] Bai, R.L.; Paull, K.D.; Herald, C.L.; Malspeis, L.; Pettit, G.R.; Hamel, E. Halichondrin B and homohalichondrin B, marine natural products binding in the vinca domain of tubulin. Discovery of tubulin-based mechanism of action by analysis of differential cytotoxicity data. *J. Biol. Chem.,* **1991**, *266*(24), 15882-15889.

[46] Hamel, E.; Covell, D.G. Antimitotic peptides and depsipeptides. *Curr. Med. Chem.-Anti-Cancer Agents,* **2002**, *2*(1), 19-53.

[47] Bai, R.; Cichacz, Z.A.; Herald, C.L.; Pettit, G.R.; Hamel, E. Spongistatin 1, a highly cytotoxic, sponge-derived, marine natural product that inhibits mitosis, microtubule assembly, and the binding of vinblastine to tubulin. *Mol. Pharmacol.,* **1993**, *44*(4), 757-766.

[48] Zhang, J.; Liu, G.; Tang, Y. Chemical function-based pharmacophore generation of selective kappa-opioid receptor agonists by catalyst and phase. *J. Mol. Model.,* **2009**, *15*(9), 1027-1041.

[49] Athar, M.; Lone, M.Y.; Khedkar, V.M.; Jha, P.C. Pharmacophore model prediction, 3D-QSAR and molecular docking studies on vinyl sulfones targeting Nrf2-mediated gene transcription intended for anti-Parkinson drug design. *J. Biomol. Struct. Dyn.,* **2016**, *34*(6), 1282-1297.

[50] SMARTS *Language for Describing Molecular Patterns, Daylight Chemical Information Systems*, Inc. Aliso Viejo, CA.

[51] Olson, E.C.; Christoffersen, R.E. *Computer-Assisted Drug Design*. American Chemical Society; Washington DC, **1979**.

[52] Wermuth, C.; Ganellin, C.; Lindberg, P.; Mitscher, L. Glossary of terms used in medicinal chemistry (IUPAC Recommendations 1998). *Pure Appl. Chem.,* **1998**, *70*(5), 1129-1143.

[53] Verma, J.; Khedkar, V.M.; Coutinho, E.C. 3D-QSAR in drug design-a review. *Curr. Top. Med. Chem.,* **2010**, *10*(1), 95-115.

[54] Bhansali, S.G.; Kulkarni, V.M. Pharmacophore generation, atom-based 3D-QSAR, docking, and virtual screening studies of p38-α mitogen activated protein kinase inhibitors: pyridopyridazin-6-ones [78] (part 2). *Res. Rep. Med. Chem.,* **2013**, *4*, 1-21.

[55] Ghosh, S.; Nie, A.; An, J.; Huang, Z. Structure-based virtual screening of chemical libraries for drug discovery. *Curr. Opin. Chem. Biol.,* **2006**, *10*(3), 194-202.

[56] Roy, K.; Chakraborty, P.; Mitra, I.; Ojha, P.K.; Kar, S.; Das, R.N. Some case studies on application of "rm2" metrics for judging quality of quantitative structure–activity relationship predictions: emphasis on scaling of response data. *J. Comput. Chem.,* **2013**, *34*(12), 1071-1082.

[57] Golbraikh, A.; Tropsha, A. Beware of q 2! *J. Mol. Graph. Model.,* **2002**, *20*(4), 269-276.

[58] Tropsha, A. Best practices for QSAR model development, validation, and exploitation. *Mol. Inform.,* **2010**, *29*(6**-**7), 476-488.

[59] Laboratory, D. *XternalValidation 1.0*, 2016.

[60] Nikolova-Jeliazkova, N.; Jaworska, J. An approach to determining applicability domains for QSAR group contribution models: an analysis of SRC KOWWIN. *Altern. Lab. Animals,* **2005**, *33*(5), 461-470.

[61] Jaworska, J.; Aldenberg, T.; Nikolova, N. Review of methods for assessing the applicability domains of SARS and QSARS. *Altern. Lab. Animals,* **2005**, *33*, 445-459.

[62] Roy, K.; Kar, S. The rm2 metrics and regression through origin approach: reliable and useful validation tools for predictive QSAR models (Commentary on 'Is regression through origin useful in external validation of QSAR models?'). *Eur. J. Pharm. Sci.,* **2014**, *62*, 111-114.

[63] Roy, K.; Kar, S.; Ambure, P. On a simple approach for determining applicability domain of QSAR models. *Chemometrics Intell. Lab. Sys.,* **2015**, *145*, 22-29.

[64] Irwin, J.J.; Shoichet, B.K. ZINC-a free database of commercially available compounds for virtual screening. *J. Chem. Info. Model.,,* **2005**, *45*(1), 177-182.

[65] Irwin, J.J.; Sterling, T.; Mysinger, M.M.; Bolstad, E.S.; Coleman, R.G. ZINC: a free tool to discover chemistry for biology. *J. Chem. Inf. Model.,* **2012**, *52*(7), 1757-1768.

[66] Bohm, H.J. The computer program LUDI: a new method for the *de novo* design of enzyme inhibitors. *J. Comput. Aided Mol. Des.,* **1992**, *6*(1), 61-78.

[67] Gigant, B.; Wang, C.; Ravelli, R.B.; Roussi, F.; Steinmetz, M.O.; Curmi, P.A.; Sobel, A.; Knossow, M. Structural basis for the regulation of tubulin by vinblastine. *Nature,* **2005**, *435*(7041), 519-522.

[68] Carlomagno, T. *Tubulin-Binding Agents: Synthetic, Structural and Mechanistic Insights*. Springer-Verlag: Berlin Heidelberg, **2009**, Vol. 286, pp. 1-27

[69] Rarey, M.; Kramer, B.; Lengauer, T.; Klebe, G. A fast flexible docking method using an incremental construction algorithm. *J. Mol. Biol.,* **1996**, *261*(3), 470-489.

[70] Schrödinger, Schrödinger Release 2014-4. *Schrödinger, LLC,* New York, NY, 2014.

[71] Bowers, K.J.; Chow, E.; Xu, H.; Dror, R.O.; Eastwood, M.P.; Gregersen, B.A.; Klepeis, J.L.; Kolossvary, I.; Moraes, M.A.; Sacerdoti, F.D. In: *SC 2006 Conference, Proceedings of the ACM/IEEE*; IEEE, **2006**, pp. 43-43.

[72] Shaw, D.E. A fast, scalable method for the parallel evaluation of distance-limited pairwise particle interactions. *J. Comput. Chem.,* **2005**, *26*(13), 1318-1328.

[73] Bowers, K.J.; Dror, R.O.; Shaw, D.E. The midpoint method for parallelization of particle simulations. *J. Chem. Phys.*, **2006**, *124*(18), 184109.

[74] Darden, T.; York, D.; Pedersen, L. Particle mesh Ewald: An N log (N) method for Ewald sums in large systems. *J. Chem. Phys.,* **1993**, *98*(12), 10089-10092.

[75] Hoover, W.G. Canonical dynamics: equilibrium phase-space distributions. *Phys. Rev. A,* **1985**, *31*(3), 1695.

[76] Kristam, R.; Parmar, V.; Viswanadhan, V.N. 3D-QSAR analysis of TRPV1 inhibitors reveals a pharmacophore applicable to diverse scaffolds and clinical candidates. *J. Mol. Graph Model.,* **2013**, *45*, 157-172.

[77] Seidel, T.; Ibis, G.; Bendix, F.; Wolber, G. Strategies for 3D pharmacophore-based virtual screening. *Drug Discov. Today: Technol.,* **2011**, *7*(4), e221-e228.

[78] Qing, X.; Lee, X.Y.; De Raeymaecker, J.; Tame, J.R.; Zhang, K.Y.; De Maeyer, M.; Voet, A. Pharmacophore modeling: advances, limitations, and current utility in drug discovery. *J. Receptor, Ligand Channel Res.,* **2014**, *7*, 81-92.

[79] Nagarajan, S.; Choi, M.J.; Cho, Y.S.; Min, S.J.; Keum, G.; Kim, S.J.; Lee, C.S.; Pae, A.N. Tubulin inhibitor identification by bioactive conformation alignment pharmacophore-guided virtual screening. *Chem. Biol. Drug Des.,* **2015**, *86*(5), 998-1016.

[80] Verma, J.; Khedkar, V.M.; Coutinho, E.C. 3D-QSAR in drug design--a review. *Curr. Top. Med. Chem.,* **2010**, *10*(1), 95-115.

[81] Tanwar, P.O.; Karthikeyan, C.; Moorthy, S.H.N.N.; Trivedi, P. 3D QSAR of aminophenyl benzamide derivatives as histone deacetylase inhibitors. *Med. Chem.,* **2010**, *6*(5), 277-285.

[82] Kaur, M.; Kumari, A.; Bahia, M.S.; Silakari, O. Designing of new multi-targeted inhibitors of spleen tyrosine kinase (Syk) and zeta-associated protein of 70kDa (ZAP-70) using hierarchical virtual screening protocol. *J. Mol. Graphics Model.,* **2013**, *39*, 165-175.

[83] Bajorath, J. Integration of virtual and high-throughput screening. *Nat. Rev. Drug Discov.,* **2002**, *1*(11), 882-894.

[84] Athar, M.; Lone, M.Y.; Jha, P.C. First protein drug target's appraisal of lead-likeness descriptors to unfold the intervening chemical space. *J. Mol. Graphics Model.,* **2017**, *72*, 272-282.

[85] QikProp *Schrödinger, LLC,* New York, NY, 4.2; 2014.

[86] Lipinski, C.A.; Lombardo, F.; Dominy, B.W.; Feeney, P.J. Experimental and computational approaches to estimate solubility and permeability in drug discovery and development settings. *Adv. Drug Deliv. Rev.,* **2012**, *64*, 4-17.

[87] Veber, D.F.; Johnson, S.R.; Cheng, H.-Y.; Smith, B.R.; Ward, K.W.; Kopple, K.D. Molecular properties that influence the oral bioavailability of drug candidates. *J. Med. Chem.,* **2002**, *45*(12), 2615-2623.

[88] Cormier, A.; Knossow, M.; Wang, C.; Gigant, B. In *Methods in Cell Biology*. Leslie, W.; John, J.C. Eds.; Academic Press: Cambridge, MA, **2010**; Vol. *95*, pp. 373-390.

[89] Cormier, A.; Marchand, M.; Ravelli, R.B.; Knossow, M.; Gigant, B. Structural insight into the inhibition of tubulin by vinca domain peptide ligands. *EMBO Reports,* **2008**, *9*(11), 1101-1106.

[90] Laskowski, R.A. PDBsum: summaries and analyses of PDB structures. *Nucleic Acids Res.,* **2001**, *29*(1), 221-222.

[91] Chopra, A.; Anderson, A.; Giardina, C. Novel piperazine-based compounds inhibit microtubule dynamics and sensitize colon

cancer cells to tumor necrosis factor-induced apoptosis. *J. Biol. Chem.,* **2014**, *289*(5), 2978-2991.

[92] Reulecke, I.; Lange, G.; Albrecht, J.; Klein, R.; Rarey, M. Towards an integrated description of hydrogen bonding and dehydration: decreasing false positives in virtual screening with the HYDE scoring function. *ChemMedChem,* **2008**, *3*(6), 885-897.

[93] Schneider, N.; Hindle, S.; Lange, G.; Klein, R.; Albrecht, J.; Briem, H.; Beyer, K.; Claußen, H.; Gastreich, M.; Lemmen, C. Substantial improvements in large-scale redocking and screening using the novel HYDE scoring function. *J. Computer-Aided Mol. Design,* **2012**, *26*(6), 701-723.

[94] Lyne, P.D. Structure-based virtual screening: an overview. *Drug Discov. Today,* **2002**, *7*(20), 1047-1055.

[95] Jorgensen, W.L. The many roles of computation in drug discovery. *Science,* **2004**, *303*(5665), 1813-1818.